The Astrophysical Journal Letters, 732:L35 (6pp), 2011 May 10 doi:10.1088/2041-8205/732/2/L35

DISCOVERY OF A MULTIPLY LENSED SUBMILLIMETER GALAXY IN EARLY HerMES *HERSCHEL*/SPIRE* DATA

A. Conley[1], A. Cooray[2,3], J. D. Vieira[3], E. A. González Solares[4], S. Kim[2], J. E. Aguirre[5], A. Amblard[2], R. Auld[6], A. J. Baker[7], A. Beelen[8], A. Blain[3], R. Blundell[9], J. Bock[3,10], C. M. Bradford[3,10], C. Bridge[3], D. Brisbin[11], D. Burgarella[12], J. M. Carpenter[3], P. Chanial[13], E. Chapin[14], N. Christopher[15], D. L. Clements[16], P. Cox[17], S. G. Djorgovski[3], C. D. Dowell[3,10], S. Eales[6], L. Earle[1], T. P. Ellsworth-Bowers[18], D. Farrah[19], A. Franceschini[20], D. Frayer[21], H. Fu[3], R. Gavazzi[22], J. Glenn[1,18], M. Griffin[6], M. A. Gurwell[9], M. Halpern[14], E. Ibar[23], R. J. Ivison[24,25], M. Jarvis[25], J. Kamenetzky[18], M. Krips[17], L. Levenson[3,10], R. Lupu[5], A. Mahabal[3], P. D. Maloney[1], C. Maraston[26], L. Marchetti[20], G. Marsden[14], H. Matsuhara[27], A. M. J. Mortier[16], E. Murphy[3,28], B. J. Naylor[10], R. Neri[17], H. T. Nguyen[10,3], S. J. Oliver[19], A. Omont[21], M. J. Page[29], A. Papageorgiou[6], C. P. Pearson[30,31], I. Pérez-Fournon[32,33], M. Pohlen[6], N. Rangwala[1], J. I. Rawlings[29], G. Raymond[6], D. Riechers[3,36], G. Rodighiero[20], I. G. Roseboom[19], M. Rowan-Robinson[16], B. Schulz[3,28], Douglas Scott[14], K. Scott[5], P. Serra[2], N. Seymour[29], D. L. Shupe[3,28], A. J. Smith[19], M. Symeonidis[29], K. E. Tugwell[29], M. Vaccari[20], E. Valiante[14], I. Valtchanov[34], A. Verma[15], M. P. Viero[3], L. Vigroux[22], L. Wang[19], D. Wiebe[14], G. Wright[23], C. K. Xu[3,28], G. Zeimann[35], M. Zemcov[3,10], and J. Zmuidzinas[3,10]

[1] Center for Astrophysics and Space Astronomy, 389 UCB, University of Colorado, Boulder, CO 80309, USA; alexander.conley@colorado.edu

[2] Department of Physics & Astronomy, University of California, Irvine, CA 92697, USA

[3] California Institute of Technology, 1200 E. California Blvd., Pasadena, CA 91125, USA

[4] Institute of Astronomy, University of Cambridge, Madingley Road, Cambridge CB3 0HA, UK

[5] Department of Physics and Astronomy, University of Pennsylvania, Philadelphia, PA 19104, USA

[6] Cardiff School of Physics and Astronomy, Cardiff University, Queens Buildings, The Parade, Cardiff CF24 3AA, UK

[7] Department of Physics and Astronomy, Rutgers, The State University of New Jersey, 136 Frelinghuysen Rd, Piscataway, NJ 08854, USA

[8] Institut d'Astrophysique Spatiale (IAS), bâtiment 121, Université Paris-Sud 11 and CNRS (UMR 8617), 91405 Orsay, France

[9] Harvard-Smithsonian Center for Astrophysics, 60 Garden Street, Cambridge, MA 02138, USA

[10] Jet Propulsion Laboratory, 4800 Oak Grove Drive, Pasadena, CA 91109, USA

[11] Space Science Building, Cornell University, Ithaca, NY 14853-6801, USA

[12] Laboratoire d'Astrophysique de Marseille, OAMP, Université Aix-marseille, CNRS, 38 rue Frédéric Joliot-Curie, 13388 Marseille cedex 13, France

[13] Laboratoire AIM-Paris-Saclay, CEA/DSM/Irfu-CNRS-Université Paris Diderot, CE-Saclay, pt courrier 131, F-91191 Gif-sur-Yvette, France

[14] Department of Physics & Astronomy, University of British Columbia, 6224 Agricultural Road, Vancouver, BC V6T 1Z1, Canada

[15] Department of Astrophysics, Denys Wilkinson Building, University of Oxford, Keble Road, Oxford OX1 3RH, UK

[16] Astrophysics Group, Imperial College London, Blackett Laboratory, Prince Consort Road, London SW7 2AZ, UK

[17] Institut de RadioAstronomie Millimétrique, 300 Rue de la Piscine, Domaine Universitaire, 38406 Saint Martin d'Hères, France

[18] Department of Astrophysical and Planetary Sciences, CASA 389-UCB, University of Colorado, Boulder, CO 80309, USA

[19] Astronomy Centre, Department of Physics & Astronomy, University of Sussex, Brighton BN1 9QH, UK

[20] Dipartimento di Astronomia, Università di Padova, vicolo Osservatorio, 3, 35122 Padova, Italy

[21] NRAO, P.O. Box 2, Green Bank, WV 24944, USA

[22] Institut d'Astrophysique de Paris, UMR 7095, CNRS, UPMC Université Paris 06, 98bis boulevard Arago, F-75014 Paris, France

[23] UK Astronomy Technology Centre, Royal Observatory, Blackford Hill, Edinburgh EH9 3HJ, UK

[24] Institute for Astronomy, University of Edinburgh, Royal Observatory, Blackford Hill, Edinburgh EH9 3HJ, UK

[25] Centre for Astrophysics Research, University of Hertfordshire, College Lane, Hatfield, Hertfordshire AL10 9AB, UK

[26] Institute of Cosmology and Gravitation, University of Portsmouth, Dennis Sciama Building, Burnaby Road, Portsmouth PO1 3FX, UK

[27] Institute for Space and Astronautical Science, Japan Aerospace and Exploration Agency, Sagamihara, Kanagawa 229-8510, Japan

[28] Infrared Processing and Analysis Center, MS 100-22, California Institute of Technology, JPL, Pasadena, CA 91125, USA

[29] Mullard Space Science Laboratory, University College London, Holmbury St. Mary, Dorking, Surrey RH5 6NT, UK

[30] Space Science & Technology Department, Rutherford Appleton Laboratory, Chilton, Didcot, Oxfordshire OX11 0QX, UK

[31] Institute for Space Imaging Science, University of Lethbridge, Lethbridge, Alberta, T1K 3M4, Canada

[32] Instituto de Astrofísica de Canarias (IAC), E-38200 La Laguna, Tenerife, Spain

[33] Departamento de Astrofísica, Universidad de La Laguna (ULL), E-38205 La Laguna, Tenerife, Spain

[34] Herschel Science Centre, European Space Astronomy Centre, Villanueva de la Cañada, 28691 Madrid, Spain

[35] University of California, 1 Shields Avenue, Davis, CA 95616, USA

Received 2011 February 1; accepted 2011 April 8; published 2011 April 21

ABSTRACT

We report the discovery of a bright (f (250 μm) $>$ 400 mJy), multiply lensed submillimeter galaxy HERMES J105751.1+573027 in *Herschel*/SPIRE Science Demonstration Phase data from the HerMES project. Interferometric 880 μm Submillimeter Array observations resolve at least four images with a large separation of $\sim$9″. A high-resolution adaptive optics K_p image with Keck/NIRC2 clearly shows strong lensing arcs. Follow-up spectroscopy gives a redshift of $z = 2.9575$, and the lensing model gives a total magnification of $\mu \sim 11 \pm 1$. The large image separation allows us to study the multi-wavelength spectral energy distribution (SED) of the lensed source unobscured by the central lensing mass. The far-IR/millimeter-wave SED is well described by a modified blackbody fit with an unusually warm dust temperature, 88 ± 3 K. We derive a lensing-corrected total IR luminosity of $(1.43 \pm 0.09) \times 10^{13}\ L_{\odot}$, implying a star formation rate of $\sim$2500 $M_{\odot}$ yr^{-1}. However, models primarily developed from brighter galaxies selected at longer wavelengths are a poor fit to the full optical-to-millimeter SED. A number

of other strongly lensed systems have already been discovered in early *Herschel* data, and many more are expected as additional data are collected.

Key words: galaxies: high-redshift – galaxies: starburst – gravitational lensing: strong – submillimeter: galaxies

Online-only material: color figure

1. INTRODUCTION

The discovery of a population of high-redshift, prodigiously star-forming galaxies at submillimeter wavelengths has revolutionized our understanding of cosmological star formation (e.g., Blain et al. 2002; Chapman et al. 2005). These submillimeter galaxies (SMGs) are frequently faint at optical wavelengths due to significant extinction, but some have far-infrared luminosities in excess of $10^{13}\,L_{\odot}$, and are forming stars at $>1000\,M_{\odot}\,\mathrm{yr}^{-1}$. They are believed to be the progenitors of nearby massive elliptical galaxies (Swinbank et al. 2008), yet many of their properties remain mysterious.

Dusty, star-forming galaxies are responsible for most of the cosmic infrared background (CIB, e.g., Marsden et al. 2009; Glenn et al. 2010), which contains as much energy as all of the optical light ever emitted by galaxies (Puget et al. 1996). Modelers have had some success in fitting the spectral energy distributions (SEDs) of SMGs and using this to infer their properties (e.g., Rowan-Robinson et al. 2008), but it is difficult to study the sources that produce the CIB in detail because they are individually faint. These efforts are biased toward extremely luminous, red galaxies by selection effects, so it is interesting to test how well such models describe the less luminous *Herschel* sources selected at shorter wavelengths.

Confusion noise generally sets the flux limit at which individual *Herschel* sources can be studied. Gravitational lensing allows this limit to be circumvented. Due to the rapidly rising source counts at faint flux densities (Glenn et al. 2010) and the negative *K*-correction at submillimeter wavelengths, strong lensing is expected to be relatively common for SMGs (Blain 1996). Indeed, follow-up of early Spectral and Photometric Imaging Receiver (SPIRE) data has shown that a large fraction of the brightest sources are lensed by other galaxies (Negrello et al. 2010). Vieira et al. (2010) discovered a population of bright galaxies at 1.4 and 2 mm, and suggested that these are lensed. Lensing allows us to study the properties of intrinsically fainter SMGs at a level of detail that is currently difficult otherwise (Swinbank et al. 2010; Ivison et al. 2010b). Galaxy–galaxy lensing is expected to dominate, with generally small image separations, so emission and absorption associated with the foreground lens may obscure the SMG in the optical and near-IR; this is the case for all of the sources in Negrello et al. (2010).

Here we report the discovery of an SMG system (HERMES J105751.1+573027, hereafter HLSW-01) multiply lensed by a group of galaxies at $z = 2.9575 \pm 0.0001$ in Science Demonstration Phase *Herschel*/SPIRE observations of the Lockman-SWIRE field as part of the *Herschel* Multi-tiered Extragalactic Survey (HerMES; S. Oliver et al. 2011, in preparation), with coordinates $\alpha = 10^{\mathrm{h}}57^{\mathrm{m}}51^{\mathrm{s}}\delta = 57^{\circ}30'27''$ (J2000). A number of additional lensed systems are already known in HerMES data. The large separation between the images allows us to measure the SED of this object across a long wavelength baseline. In this Letter, we model the optical-to-millimeter SED of this object. The lensing model for this system, based on high-resolution optical and near-IR observations, is presented in Gavazzi et al. (2011, hereafter G11). We have also obtained high-resolution CO line maps (Riechers et al. 2010, hereafter R11) and used the CO line strength distribution to model the molecular gas (Scott et al. 2011, hereafter S11).

2. OBSERVATIONS

HLSW-01 was discovered using observations with the SPIRE (Griffin et al. 2010) on board *Herschel* (Pilbratt et al. 2010). It was selected for further follow-up with Z-Spec, a millimeter-band grating spectrograph at the Caltech Sub-mm Observatory (Earle et al. 2006), based on its brightness and blue color ($f\,(500\,\mu\mathrm{m}) < f\,(300\,\mu\mathrm{m})$); the latter was intended to avoid $z > 4$ sources where a redshift would be difficult to obtain. Z-Spec gives a secure redshift of $z = 2.958 \pm 0.007$ (S11). R11 use additional CO lines measured with the Plateau de Bure Interferometer (PdBI), the Combined Array for Research in Millimeter-wave Astronomy (CARMA), and Zpectrometer on the Green Bank Telescope to refine the redshift, yielding $z = 2.9575 \pm 0.0001$.

HLSW-01 is unresolved in the diffraction-limited SPIRE observations ($\mathrm{FWHM}_{250\,\mu\mathrm{m}} = 18\farcs6$). The extreme brightness ($f\,(250\,\mu\mathrm{m}) \simeq 400\,\mathrm{mJy}$) and the morphology in the optical and near-IR suggested a lensed source. A Subaru *i* image from the SERVS survey[37] shows clear evidence of lensing. The source is visible in previously obtained *gr* WHT observations and in data from the *Spitzer*/SWIRE survey (J. A. Surace et al. 2011, in preparation). We obtained observations with the Submillimeter Array (SMA) in compact configuration at 880 μm (beam FWHM $2\farcs3$), resolving the source into at least four components matching the position of several optical sources and surrounding a foreground elliptical galaxy. We further obtained a K_p adaptive optics (AO) observation using NIRC2 on the Keck II telescope and the laser guide star system (Wizinowich et al. 2006). PdBI CO maps, presented in R11, detect at least the two brightest sources and show that they are at the same redshift. The photometric redshift of the central elliptical is 0.60 ± 0.04 (Oyaizu et al. 2008). An optical spectrum obtained with the double spectrograph on the Hale telescope has absorption features consistent with the photo-z.

The numbering scheme used to identify sources in this Letter is shown in Figure 1, along with a montage of observations at multiple wavelengths. The high-resolution K_p image was used to construct a lensing model, which was compared with the *i* and PdBI observations to constrain differential magnification (see G11 for details). This model has five lensing masses at the locations of foreground galaxies and gives a total magnification factor of $\mu = 10.86 \pm 0.68$ for all five detected images based

* *Herschel* is an ESA space observatory with science instruments provided by European-led principal Investigator consortia and with important participation from NASA.

[36] Hubble Fellow.

[37] http://www.cv.nrao.edu/∼mlacy/servs.html

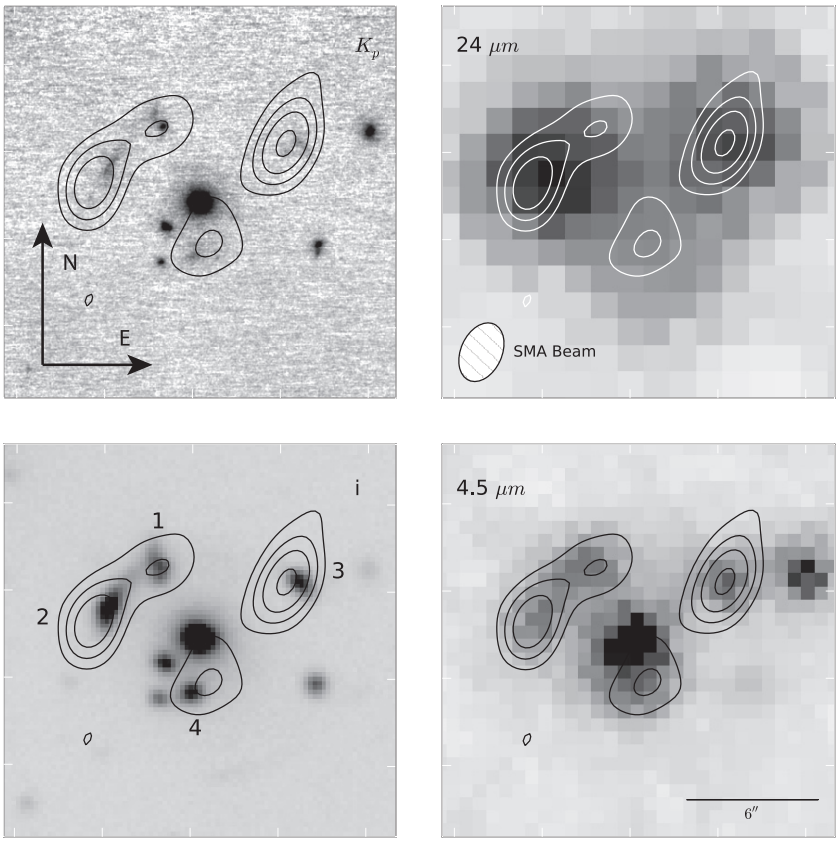

Figure 1. Composite of selected multi-wavelength observations of HLSW-01. Each image is 18″ × 18″. Clockwise from the upper left: Keck K_p AO image; *Spitzer*/MIPS 24 μm; *Spitzer*/IRAC 4.5 μm; Subaru SuprimeCam *i*. In all panels the contours show the SMA 880 μm observations. The numbering scheme used to identify sources in this Letter is shown in the bottom left panel. The highest resolution *Herschel*/SPIRE passband has a resolution of 18.″6, larger than the entire field shown here.

on a cored-isothermal model. The velocity dispersion strongly suggests that the lenses reside in a massive group of galaxies.

The photometry is summarized in Table 1. At optical wavelengths the individual images are blended and partially resolved, so neither point-spread function (PSF) nor aperture photometry is entirely satisfactory. We use aperture photometry with a relatively small aperture radius to minimize blending and compute the aperture corrections for the partially resolved sources by convolving the lens model to the matching resolution in each band; the adjustment to the aperture correction compared with isolated point sources is only a few percent. We exclude photometry of image 1 because it is contaminated by a foreground object, and again use the lensing model to correct for the omitted light, which is a ∼15% correction.

In the *Spitzer*/SWIRE data, the individual images are separable in the Infrared Array Camera (IRAC) bands (3.6 to 8 μm), and the SWIRE PSF photometry is adequate for our purposes. We use only photometry of sources 2 and 3, again using the lensing model to correct for the omitted sources 1 and 4. HLSW-01 is not present in the SWIRE catalog at 3.6 μm. The FWHM of the 70 and 160 μm MIPS observations are much larger than the separation between individual images, so the catalog flux measurement already includes all the images. At 24 μm the SWIRE aperture is just smaller than the separation, so we re-measured the photometry using a larger aperture.

The SPIRE fluxes used here are from the HerMES SCATv3.1 catalog (A. J. Smith et al. 2011, in preparation). For the SMA data we extract photometry and positions using the CASA[38]

[38] http://casa.nrao.edu

Table 1
Photometry

Wavelength (μm)	Flux Density	Telescope/Detector
0.48 (*g*)	26.0 ± 0.3 μJy	INT/WFC
0.63 (*r*)	46.5 ± 0.6 μJy	INT/WFC
0.76 (*i*)	47.9 ± 0.3 μJy	Subaru/SuprimeCam
2.2 (K_p)	63.1 ± 2.0 μJy	Keck II/NIRC2
4.5	376 ± 6 μJy	*Spitzer*/IRAC
5.8	442 ± 11 μJy	*Spitzer*/IRAC
8.0	558 ± 16 μJy	*Spitzer*/IRAC
24	5.5 ± 0.4 mJy	*Spitzer*/MIPS
72	22.2 ± 3 mJy	*Spitzer*/MIPS
160	310 ± 8 mJy	*Spitzer*/MIPS
250	425 ± 10 mJy	*Herschel*/SPIRE
350	340 ± 10 mJy	*Herschel*/SPIRE
510	233 ± 11 mJy	*Herschel*/SPIRE
880	52.8 ± 0.5 mJy	SMA
1000–1100	27.5 ± 0.6 mJy	CSO/Z-Spec
1100–1200	20.4 ± 0.5 mJy	CSO/Z-Spec
1200–1300	16.2 ± 0.5 mJy	CSO/Z-Spec
1300–1400	12.0 ± 0.5 mJy	CSO/Z-Spec
1400–1500	9.9 ± 0.6 mJy	CSO/Z-Spec
3400	0.61 ± 0.19 mJy	CARMA
214000	1.8 ± 0.7 mJy	VLA

Notes. Combined flux densities for all the detected images as detailed in the text. For brevity, only the summed flux density from all images is provided. All values are calibrated relative to an F_ν = const SED. Note that calibration errors, which are dominant at most wavelengths and are strongly correlated between points, are not included, and neither are contamination/confusion errors. These values have not been corrected for magnification.

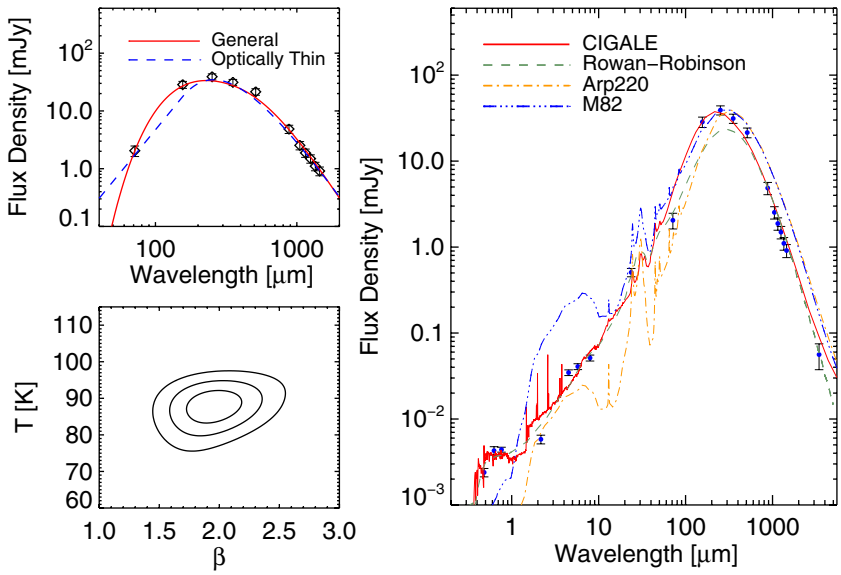

Figure 2. SED fits to HLSW-01 after correction for flux magnification. The left-hand panels show the modified blackbody fits to the long-wavelength observations (top panel) and the constraints on the temperature and β (the contours correspond to 68%/95%/99% enclosed probability) for the general form of the model. Note that the data points are strongly correlated, and the optically thick fit is an excellent match to the data. The right-hand panel compares the optical-to-millimeter SED compared with the best-fitting `CIGALE` model, the best combination of templates from Rowan-Robinson et al. (2010), and the IR SEDs of Arp220 and M82 (prototypical nearby IR-luminous galaxies) scaled to have the same maximum flux density. All wavelengths are observer frame.

(A color version of this figure is available in the online journal.)

`imfit` task. For Z-Spec, we bin the spectrum into five 100 μm bins after masking noisy channels and the detected CO lines. The 20 cm photometry is from the FIRST survey (Becker et al. 1995).

We place upper limits on the potential foreground contamination by scaling the observed elliptical galaxy SEDs from Dale et al. (2007) and Temi et al. (2007) to match the optical magnitudes of the central lensing elliptical, taking the highest resulting fluxes in each band as our contamination limit. This is not relevant at shorter wavelengths where the sources are clearly resolved. The potential contamination peaks at 6 mJy at 160 μm and 3 mJy at 70 μm. Given the SED, only the potential 70 μm contamination is significant, but we adopt the contamination limits as an additional correlated uncertainty at all wavelengths. We take calibration errors, which also affect the photometry in a correlated fashion, from the instrument documentation.

3. SED FITTING AND SOURCE PROPERTIES

We first analyze the SED by fitting simple modified blackbody models to the long-wavelength data. It is possible that the far-IR emission has a different spatial distribution than the shorter-wavelength data used to derive the lensing model, but the current SMA observations are not high enough resolution to explore this issue. Therefore, we assume that the near- and far-IR emission are co-located. G11 find evidence for a small shift ($\sim$0.″4) between the PdBI CO emission and the optical emission, too small to significantly affect our results.

The standard form for a modified blackbody SED is a frequency-dependent optical depth factor: $f_\nu \propto (1 - \exp[-\tau(\nu)])B_\nu(T)$, where B_ν is the Planck function. The optical depth is assumed to be a power law in frequency, $\tau = (\nu/\nu_0)^\beta$ following Draine (2006). $\lambda_0 = c/\nu_0$ is the wavelength where the optical depth is unity. In the optically thin case, $\nu \ll \nu_0$, this reduces to $f_\nu \propto \nu^\beta B_\nu(T)$. The latter is often used in the literature to estimate temperatures, but here our data allow us to drop the assumption of optical thinness. In both cases we join the modified blackbody to a simple power law on the blue side of the peak (Blain et al. 2003), which only affects the 70 μm observation.

Table 2
Modified Blackbody Fits

Model	General: $1 - e^{-\tau}$	Optically Thin: ν^β
T	88.0 ± 2.9 K	48.5 ± 2.6 K
β	1.95 ± 0.14	1.61 ± 0.15
λ_0	197 ± 19 μm	NA
$L_{\rm IR}$	$(1.43 \pm 0.09) \times 10^{13}$ $L_\odot$	$(1.13 \pm 0.09) \times 10^{13}$ $L_\odot$
SFR	2460 ± 160 $M_\odot$ yr^{-1}	1950 ± 160 $M_\odot$ yr^{-1}
χ^2	6.77 for 6 dof	22.1 for 7 dof

Notes. Fit values for the two modified blackbody models, applied to the magnification corrected 70–1500 μm photometry. The second model assumes optically thin emission and is only presented for comparison with literature values. The derived parameters include the uncertainty in the magnification. For $L_{\rm IR}$, we assume $h = 0.7$, $\Omega_m = 0.27$, and $\Omega_\Lambda = 0.73$.

We fit both models from 70 μm to 1.5 mm to derive the temperature and total IR luminosity, including the error on the magnification. The fit is shown in the left-hand panels of Figure 2 and the parameters are given in Table 2. All of the parameters are well constrained by our data. We find $\lambda_0 \simeq 200$ μm, a reasonable match to the theoretically expected value $\lambda_0 \simeq 100$ μm (Draine 2006) and similar to that derived for Arp 220 (Blain et al. 2003). The emission is optically thick bluer than observer frame $\sim$800 μm. A two-temperature model decreases the χ^2 by $<$0.002 for the optically thick model (since there is virtually no contribution from the second component for the best fit), and for the optically thin model by about 5, so the latter remains a very poor fit.

The temperatures and β values for the two different models disagree strongly; this is also the case for the fits to Arp 220 in Blain et al. (2003). The general model (i.e., $1 - \exp[-\tau]$)

fits our data quite well, but the optically thin model does not, with a reduced $\chi^2_\nu > 3$. The derived temperature for the former is fairly high (∼90 K), suggesting a dust-enshrouded active galactic nucleus (AGN) contribution. This result is robust against removing the data from any single instrument or any individual data point. Obtaining an acceptable fit for a more typical dust temperature, such as 60 K, requires increasing all the errors by a factor of >2.2, including calibration errors. It is possible that the lensing is selectively magnifying a warm component and that this high temperature is not representative of the SMG as a whole. The poor quality of the optically thin fit is similarly robust, unless the SPIRE observations are removed, in which case it becomes acceptable ($\chi^2_\nu = 1.1$). It is therefore possible that such warm SMGs have been missed in previous surveys that did not have observations near the peak of the SED, as it would then be difficult to distinguish between the optically thin and thick cases. Since the general model fits the data much better, and makes fewer assumptions, henceforth we only discuss the results of this fit.

The above findings are independent of the lensing model, unless the location of the emission (and hence the magnification) changes strongly from 250 μm to 1.5 mm, which is unlikely. Turning to quantities which must be corrected for the lensing magnification, we find a far-IR luminosity of $L_{\rm IR} = 1.43 \times 10^{13}\,L_\odot$, where $L_{\rm IR}$ is defined as the luminosity from 8 to 1000 μm in the rest frame. This implies a star formation rate of $\sim$2500 $M_\odot\,{\rm yr}^{-1}$ from the relation of Kennicutt (1998), ignoring any AGN contribution. We also measured $L_{\rm IR}$ by spline-interpolating the observations, which gives a similar value ($1.49 \times 10^{13}\,L_\odot$). Assuming a mass-absorption coefficient of $\kappa_\nu = 2.64\,{\rm m}^2\,{\rm kg}^{-1}$ at 125 μm following Dunne et al. (2003), from the temperature and luminosity we infer a dust mass of $M_d \simeq 1 \times 10^8\,M_\odot$; κ_ν, and hence M_d, is uncertain by at least a factor of three. Further assuming a molecular gas-to-dust ratio of 60 for SMGs (Coppin et al. 2008), we estimate a gas depletion time of $\sim 2.4 \times 10^6$ yr, considerably shorter than the value of $>4 \times 10^7$ yr for "typical" SMGs derived by, e.g., Daddi et al. (2010); see R11 for actual gas mass estimates.

This source is weakly detected at 1.4 GHz in the FIRST survey, so we also compute $q_{\rm IR}$, which is the logarithmic ratio of $L_{\rm IR}$ and the rest-frame 1.4 GHz flux density. HLSW-01 has an moderately low ratio, $q_{\rm IR} = 1.5 \pm 0.2$, compared with the mean value and scatter of $q_{\rm IR} = 2.4 \pm 0.12$ for HerMES sources with firm radio cross-identifications (Ivison et al. 2010a), although not the lowest found. The high 1.4 GHz flux density suggests some AGN contribution. However, the 5″ resolution of the FIRST survey is not good enough to rule out foreground contamination. While this is likely small, $q_{\rm IR}$ should be regarded as a lower limit.

In addition to the above simple models, we have also investigated a variety of template fits across all wavelengths using several packages. A similar study was carried out for isolated, but somewhat intrinsically brighter, *Herschel* sources by Brisbin et al. (2010), who found that model templates were generally a good match to the data. This is not the case here; available templates generally do not fit both the near-IR and far-IR through millimeter-wave data simultaneously. The templates of Rowan-Robinson et al. (2008, 2010) underestimate the far-IR flux by ∼30%. This is also the case for the models of Siebenmorgen & Krügel (2007). In both cases this is because the SED of HLSW-01 peaks blueward of the templates. Similarly, the models of da Cunha et al. (2008) are unable to reproduce the full SED (E. da Cunha 2010, private communication). The potential foreground contamination discussed in Section 2 is much too small to explain these issues.

Next we turn to the CIGALE package (Noll et al. 2009), which combines optical/near-IR templates with a longer wavelength dust model. Using a two-stellar population model, this fits the SED considerably better, but has some issues in the near-IR, overpredicting K_p (rest frame g) flux density by a factor of two and missing the slope of the IRAC observations. We are unable to explain this discrepancy. Ignoring these issues, CIGALE finds a total stellar mass of $\log_{10} M_* = 10.8^{+0.2}_{-0.3}$ and a star formation rate of $\log_{10}{\rm SFR} = 3.3^{+0.4}_{-0.5}$ in $M_\odot$ and $M_\odot\,{\rm yr}^{-1}$, respectively; 70% ± 30% of the stars are in a young, strongly extinguished stellar component ($A_V = 6 \pm 2$), whose age is not well constrained. A sample of SED fits is shown in Figure 2.

4. CONCLUSIONS

The unusually large image separation of HLSW-01 compared with most lensed submillimeter sources provides an opportunity to study a submillimeter galaxy at a level of detail typically only possible for more luminous sources. Due to confusion noise, this will generally not be feasible for un-lensed sources until the completion of ALMA. Detailed models of the gas and dust content based on CO emission are presented in S11 and R11.

Modified blackbody fits to the long-wavelength data (70 μm to 1.5 mm) imply a warm dust temperature of 90 K and a star formation rate of $\sim$2500 $M_\odot\,{\rm yr}^{-1}$. Compared with other SMGs, we find a short gas depletion timescale of only a few million years, assuming negligible AGN contribution to $L_{\rm IR}$. This is one of the few SMGs that have been studied across such a wide wavelength range, due to the large image separation, so it is interesting that SED fits from the optical to the millimeter are generally a fairly poor fit to the data, typically matching the short-wavelength data well but underpredicting the far-IR peak. We obtain somewhat better results with CIGALE, but it significantly overpredicts the 2 μm flux and is not a great match to the IRAC observations. It is unclear if this galaxy is simply unusual, or if the templates—which were largely derived from even brighter galaxies selected at longer wavelengths—are not a good representation of galaxies selected at wavelengths near the peak of the far-infrared background. The latter would have significant implications for the inferred history of high-z star formation. Such warm systems may have been missed by previous surveys lacking data near the peak of the SED because of the common assumption of optical thinness. Models suggest there should be a large number of strongly lensed SMGs in *Herschel* data, which is consistent with early observations (Negrello et al. 2010), so we expect to address this question soon. The variations in lensing magnification make this a promising tool to study SMGs across a wide range of intrinsic luminosities, although relatively few sources will have such a large image separation. Additional multi-wavelength observations, particularly at high resolution, would improve the SED constraints significantly.

SPIRE has been developed by a consortium of institutes led by Cardiff University (UK) and including University of Lethbridge (Canada); NAOC (China); CEA, LAM (France); IFSI, University of Padua (Italy); IAC (Spain); Stockholm Observatory (Sweden); Imperial College London, RAL, UCL-MSSL, UKATC, University of Sussex (UK); Caltech, JPL, NHSC, University of Colorado (USA). This development has been

supported by national funding agencies: CSA (Canada); NAOC (China); CEA, CNES, CNRS (France); ASI (Italy); MCINN (Spain); SNSB (Sweden); STFC (UK); and NASA (USA). The Submillimeter Array is a joint project between the Smithsonian Astrophysical Observatory and the Academia Sinica Institute of Astronomy and Astrophysics. The IRAM Plateau de Bure Interferometer is supported by INSU/CNRS (France), MPG (Germany), and IGN (Spain). The National Radio Astronomy Observatory is a facility of the National Science Foundation operated by Associated Universities, Inc. Support for CARMA construction was derived from the Gordon and Betty Moore Foundation, the Kenneth T. and Eileen L. Norris Foundation, the James S. McDonnell Foundation, the Associates of the California Institute of Technology, the University of Chicago, the states of California, Illinois, and Maryland, and the National Science Foundation. Ongoing CARMA development and operations are supported by NSF grant ATI-0838178 to CARMA, and by the CARMA partner universities. The authors thank Elisabete da Cunha for running her models for us. The *Herschel* data presented in this Letter will be released through the *Herschel* Database in Marseille, HeDaM.[39]

Facilities: *Herschel* (SPIRE), CSO (Z-Spec), Subaru (SuprimeCam), SMA, Hale (SWIFT), Keck:II (NIRC2), IRAM:Interferometer, ING:Newton (WFC), *Spitzer* (IRAC; MIPS), CARMA, VLA, GBT (Zpectrometer)

REFERENCES

Becker, R. H., White, R. L., & Hefland, D. J. 1995, ApJ, 450, 559
Blain, A. W. 1996, MNRAS, 283, 1340
Blain, A. W., Barnard, V. E., & Chapman, S. C. 2003, MNRAS, 338, 733
Blain, A. W., Smail, I., Ivison, R. J., Kneib, J.-P., & Frayer, D.-T. 2002, Phys. Rep., 369, 111
Brisbin, D., et al. 2010, MNRAS, 409, 66
Chapman, S. C., Blain, A. W., Smail, I., & Ivison, R. J. 2005, ApJ, 622, 772
Coppin, K. E. K., et al. 2008, MNRAS, 389, 45
da Cunha, E., Charlot, S., & Elbaz, D. 2008, MNRAS, 388, 1595
Daddi, E., et al. 2010, ApJ, 714, L118
Dale, D. A., et al. 2007, ApJ, 655, 863
Draine, B. T. 2006, ApJ, 636, 1114
Dunne, L., Eales, S. A., & Edmunds, M. G. 2003, MNRAS, 341, 589
Earle, L., et al. 2006, Proc. SPIE, 6275, 32
Gavazzi, R., et al. 2011, ApJ, submitted
Glenn, J., et al. 2010, MNRAS, 409, 109
Griffin, M. J., et al. 2010, A&A, 518, L3
Ivison, R. J., et al. 2010, A&A, 518, L31
Ivison, R. J., et al. 2010, A&A, 518, L35
Kennicutt, R. C., Jr. 1998, ApJ, 498, 541
Marsden, G., et al. 2009, ApJ, 707, 1729
Negrello, M., et al. 2010, Science, 330, 800
Noll, S., Burgarella, D., Giovannoli, E., Buat, V., Marcillac, D., & Muñoz-Mateos, J. C. 2009, A&A, 507, 1793
Oliver, S., et al. 2010, A&A, 518, L21
Oyaizu, H., Lima, M., Cunha, C. E., Lin, H., Frieman, J., & Sheldon, E. S. 2008, ApJ, 674, 768
Pilbratt, G. L., et al. 2010, A&A, 518, L1
Puget, J., Abergel, A., Bernard, J.-P., Boulanger, F., Burton, W. B., Desert, F.-X., & Hartmann, D. 1996, A&A, 308, L5
Riechers, D., et al. 2011, ApJL, in press
Rowan-Robinson, M., et al. 2008, MNRAS, 386, 697
Rowan-Robinson, M., et al. 2010, MNRAS, 409, 2
Scott, K. S., et al. 2011, ApJ, in press
Siebenmorgen, R., & Krügel, E. 2007, A&A, 461, 445
Swinbank, A. M., et al. 2008, MNRAS, 391, 420
Swinbank, A. M., et al. 2010, Nature, 464, 733
Temi, P., Brighenti, F., & Mathews, W. G. 2007, ApJ, 660, 1215
Vieira, J. D., et al. 2010, ApJ, 719, 763
Wizinowich, P. L., et al. 2006, PASP, 118, 297

[39] http://hedam.oamp.fr/HerMES